NON-DARCY POROUS MEDIA FLOW IN NO-SLIP AND SLIP REGIMES

by

Antonio F. MIGUEL

Geophysics Centre of Evora & Department of Physics, University of Evora, Portugal

Original scientific paper
DOI: 10.2298/TSCI100929001M

In this paper lattice-Boltzmann equation method is used to simulate non-Darcy flow in porous media. 2-D in-line and staggered arrangements of uniform cylinders have been considered. The results of a comprehensive computational evaluation are reported: the range of validity of Darcy-Forchheimer equation is investigated and correlations for macroscopic transport properties are presented (i. e., for the permeability and the inertial parameter). Our investigation covers both no-slip and the slip-flow regimes.

Key words: *porous media, non-Darcy flow, no-slip flow regime, slip-flow regime, Knudsen number, permeability, inertial parameter, lattice-Boltzmann equation method*

Introduction

Since the 1970s, computational modelling of fluid flow through porous media has increased rapidly [1, 2]. Porous media are diverse and include different scales. The flows through macro and micro-scales are not the same. As flows approach microscopic scales, increasing deviations from the well-established continuum laws are reported [3, 4]. The Knudsen number, defined as the ratio of the molecular mean free path to the characteristic length of pores, allows establishing four regimes [5]: $0 < Kn \leq 0.001$ (no-slip), $0.001 < Kn \leq \leq 0.1$ (slip), $0.1 < Kn \leq 10$ (transition), and $Kn > 10$ (free molecular, ballistic). Navier-Stokes equation is only adequate for no-slip regime and can be extended into the *slip*-flow *regime provided* the velocity slip and temperature jump boundary conditions [4, 6]. In this regard, the limit of validity of the continuum flow description is $Kn \leq 0.1$. Discrete Boltzmann models are based on a kinetic representation of the fluid dynamics, and avoid the drawbacks associated to the conventional Navier-Stokes description. Lattice-Boltzmann equation method (LBM) is appropriate for complexes geometries and covers all these four regimes (*i. e.*, is also valid for transition and free molecular regime) [7, 8]. Within the *continuum regime*, LBM has been shown to be equivalent to a finite difference approximation of the incompressible Navier-Stokes equation [8].

LBM for modelling hydrodynamics has its origins from the lattice gas cellular automata and can be directly derived by discretizing the Boltzmann equation [7, 8]. A very

* Corresponding author; e-mail: afm@uevora.pt

widely used lattice-Boltzmann model is the lattice-Bhatnagar-Gross-Krook (BGK) [9, 10]. Especially important in the high-Reynolds number simulations are also the multiple-relaxation-time lattice-Boltzmann models that offer increased numerical stability [11, 12].

Several studies demonstrate the potential of the lattice-Boltzmann algorithm for numerical simulation of fluid through porous media [13-18]. In this paper, a numerical model based on the LBM is presented for simulating flow in non-Darcy porous media. Among other outcomes, the permeability and the inertial parameter variations are examined for both non-slip and slip flow regimes.

Lattice-Boltzmann method

In the LBM, the fluid is modelled by a single-particle distribution function and the evolution of this function is governed by a lattice Boltzmann equation. Consider $f_i(r, t)$ the particle density entering at position r and time t with a velocity v_i point in direction e_i ($v_i = e_i\delta/\eta$), where i labels the lattice directions, δ is the lattice spacing, and η – the time increment. A simple and widely used lattice-Boltzmann model is governed by a collision operator of the lattice-Bhatnagar-Gross-Krook model, based on a single collision relaxation to the local equilibrium distribution [9, 10]. The evolution equation is:

$$f_i(r + e_i\delta, t + \eta) - f_i(r, t) = -\frac{f_i(r,t) - f_i^{(0)}(r,t)}{\tau} \tag{1}$$

Here τ is the non-dimensional relaxation-time parameter, $f_i^{(0)}$ – the equilibrium distribution function, and $[f_i(r, t) - f_i^{(0)}(r, t)]/\tau$ is the collision operator very often represented by Ω_i. A solution to this equation is found by using the Chapman-Enskog expansion [19], which is much known in statistical mechanics for deriving macroscopic laws for relevant physical quantities when the Boltzmann equation is known [20]. Considering that lattice spacing and time increment (*i. e.*, δ and η) are small compared to the characteristic length and time scales, eq. (1) can be expanded around r and t. Therefore:

$$\eta\partial_t f_i + \delta(e_i\nabla)f_i + \frac{\eta^2}{2}\partial_t^2 f + \frac{\delta^2}{2}(e_i\nabla)^2 f_i + \delta\eta(e_i\nabla)\partial_t f_i = \Omega_i \tag{2}$$

The Chapman-Enskog method [19] allow us to obtain the following perturbation expansion:

$$f_i = f_i^{(0)} + \vartheta f_i^{(1)} + \vartheta^2 f_i^{(2)} + ... \tag{3}$$

where ϑ is a very small parameter [19]. To determine the terms of this expansion it is assumed that the macroscopic quantities ρ and ρu are described by the zeroth order terms [21]:

$$\rho = \sum_i f_i^{(0)}, \quad \rho u = \sum_i v_i f_i^{(0)} \tag{4}$$

To obtain a solution for eq. (1) by the eq. (3), the lattice and the equilibrium distribution are required. Figure 1 shows the Cartesian lattice with 8 velocities vectors. The central point ○ represents a particle at rest. This 2-D model is known as D2Q9 (*i. e.*, D2

denotes the 2-D of the lattice and Q9 the 9 links per lattice point). The equilibrium function is defined by [9, 10]:

$$f_i^{(0)} = a_w \rho \left(1 + 3\frac{e_i v}{v_s^2} + \frac{9}{2}\frac{(e_i v)^2}{v_s^4} - \frac{3}{2}\frac{v^2}{v_s^2} \right) \qquad (5)$$

where v_s is the propagation speed on the lattice (1 lattice spacing/time step), and a_w – 4/9, 1/9, and 1/36 for the rest particle, the particles moving to the nearest and next-nearest neighbour sites, respectively.

Under the assumption of a low Mach number, this previous formulation allows us to recover the incompressible Navier-Stokes equations with the equivalent viscosity, ν, described by [8]:

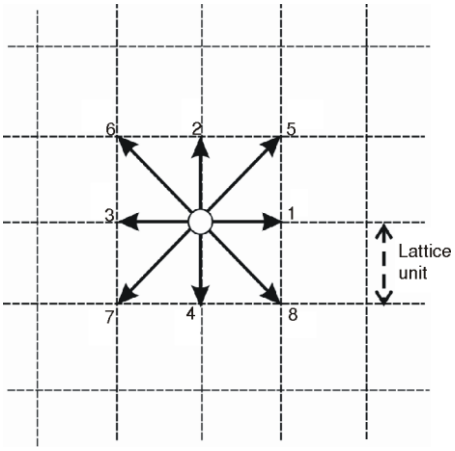

Figure 1. Discrete lattice velocities for the D2Q9 model

$$\nu = c_s^2(\tau - 0.5)\eta \qquad (6)$$

where c_s is the sound speed and η – the time increment. This equation requires that $\tau > 0.5$ and cannot be greater than 2 in order to maintain numerical stability. A detailed description of the all methodology is provided by [9, 10, 19].

Correlating the parameter τ with Knudsen number, Kn, is essential [9, 10]. As mentioned, the Knudsen number is defined as the ratio between the mean free path and the characteristic length of the pores, and regarding the degree of rarefaction there are the following regimes [5]: $0 < \mathrm{Kn} \leq 0.001$ (no-slip), $0.001 < \mathrm{Kn} \leq 0.1$ (slip), $0.1 < \mathrm{Kn} \leq 10$ (transition) and $\mathrm{Kn} > 10$ (free molecular). This study is focused on no-slip and slip flow regimes ($0 < \mathrm{Kn} \leq 0.1$). For an ideal gas the mean free path, l, is related to the equivalent viscosity, ν, and the molecular velocity, u_{mol}, as [5]:

$$\nu = 0.5 u_{mol} l \quad \text{or} \quad l = \frac{2\nu}{u_{mol}} \qquad (7)$$

Here the viscosity is given by eq. (6). From the kinetic theory of gases, the mean molecular velocity can be obtained by:

$$u_{mol} = \sqrt{\frac{8k_B T}{\pi m}} \qquad (8)$$

and

$$c_s^2 = \frac{p}{\rho} = \frac{k_B T}{m} \qquad (9)$$

where m represents the molecular mass, k_B is the Boltzmann constant, and ρ – the density. Substituting eqs. (7) to (9) into the Knudsen number equation yields:

$$\mathrm{Kn} = \frac{2\nu}{u_{mol} d} \quad \text{and} \quad \tau = \frac{\sqrt{6}\chi \mathrm{Kn}}{\sqrt{\pi}} + 0.5 \qquad (10)$$

Here Kn is the local Knudsen number and χ – the lattice number in the geometry. Since, the mean free path is inversely proportional to the pressure, the local Kn can be calculated by:

$$\mathrm{Kn} = \mathrm{Kn}_\mathrm{o} \frac{p_\mathrm{o}}{p} \tag{11}$$

where p is the pressure and the subscript o means outlet.

Geometry, boundary conditions and numerical method validation

Figure 2. 2-D porous space with in-line (l. h. s.) and staggered (r. h. s.) arrangements

Our topological space is based on uniformly distributed cylinders in 2-D for in-line and staggered arrangements (fig. 2). For the arrangements displayed in fig. 2, flow is blocked for porosities less than 0.2146 and 0.0932, respectively. Therefore, in the simulations the porosity ϕ is prescribed for higher values: $0.25 \leq \phi \leq 0.95$ for in-line arrangements and $0.20 \leq \phi \leq 0.95$ for staggered arrangements.

Simulations are performed in the Reynolds number range of 0.004-400. A periodic boundary condition is imposed at respective boundaries, while a pressure difference is prescribed between the inlet and outlet. Details of the computational procedure can be obtained in [22].

The numerical method proposed here was validated against the results presented by Serrenho and Miguel [23] for 2-D staggered arrangements (porosities 0.50 and 0.95). The deviation between our results and those presented by [23] was always less than 7%. Therefore, the numerical method is able to simulate adequately the considered flows.

Non-Darcy flow in porous media: friction factor *vs.* Reynolds number and Forchheimer number

Non-Darcy flow in porous media occurs if the Reynolds number becomes large enough so that Darcy's law, a linear relationship between fluid velocity and pressure drop (*i. e.*, shear stress is proportional to the velocity gradient inside a pore), is no longer sufficient [24]. Macroscopically, a non-linear relation between the pressure drop and the flow velocity is observed, and the Darcy-Forchheimer equation can be applied [24]. This equation is often rearranged in a dimensionless form [23, 25]:

$$f_\mathrm{K} = \frac{1}{\mathrm{Re}_\mathrm{K}} + \lambda \tag{12}$$

with

$$f_\mathrm{K} = \frac{\Delta p}{L}\frac{\sqrt{K}}{\rho u^2}, \quad \mathrm{Re}_\mathrm{k} = \frac{\rho u\sqrt{K}}{\mu}, \quad \lambda = \beta\sqrt{K} \tag{13}$$

where f_K represents the friction factor, Re_K – the Reynolds number based on permeability, λ – the a dimensionless inertia parameter, β – the inertial coefficient, u – the superficial fluid velocity, p – the pressure, ρ – the density, L – the thickness of the porous media, and K – the permeability which represents the ability of the material to transmit fluid through itself.

The dimensionless form of the Darcy-Forchheimer equation can be also presented in terms of the Forchheimer number, Fo_K (defined as the product of the Reynolds number, Re_K, by the dimensionless inertia parameter, λ), and may be written as [23, 25]:

$$f_K = \lambda\left(\frac{1}{Fo_K} + 1\right) \tag{14}$$

Experimental and numerical data from a variety of porous media has been successfully correlated with these equations [2]. In this study, eqs (13) and (14) will be used to fit the results of our computational simulations.

Results

In the following we present and analyse the results of the flow simulations in the geometries depicted in fig. 2. We apply the dimensionless forms of Darcy-Forchheimer equation (*i.e.*, eqs. 13 or 14) as phenomenological models to correlate the variations of the friction factor for different porosities and flow conditions.

No-slip flow ($0 < Kn \leq 0.001$): permeability and inertial parameter

Based on the velocity and pressure results of the simulations, the permeability and the inertia parameter was estimated and then the friction factor, the Reynolds number and the Forchheimer number calculated. The friction factor is then plotted in terms of Re_K or Fo_K. Figures 3 and 4 show the results of simulations performed with in-line and staggered porous structures for a porosity of 0.3 and 0.6, respectively.

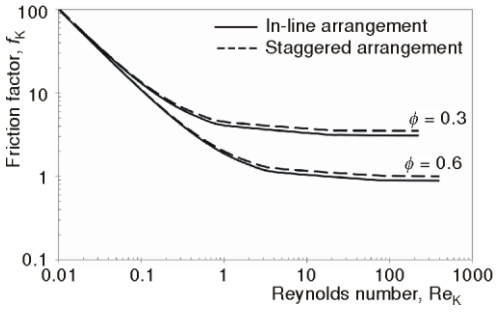

Figure 3. Logarithmic plot showing the dependence of the friction factor f_K on the Reynolds number

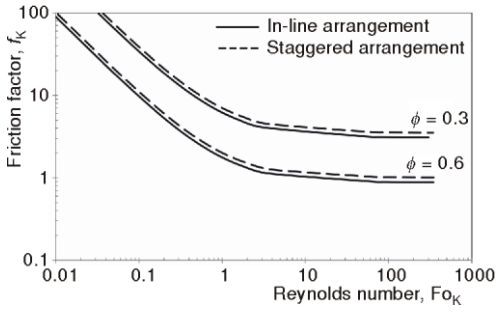

Figure 4. Logarithmic plot showing the dependence of the friction factor f_K on the Forchheimer number

In agreement with a large number of experimental and computational studies [1, 2], we also observe a transition from linear (Darcy or creeping flow regime) to non-linear (Forchheimer) regime. Figures 3 and 4 show that this transition occurs at Re_K in the range of

0.2-0.4 or Fo_K in the range of 0.3-0.7, respectively. In both plots the transition from linear to non-linear behaviour is gradual and takes place already under laminar flow regime. This means that the inertia effects (Forchheimer regime) flatten the f_K curve in a manner reminiscent of the friction factor in turbulent flow over a surface.

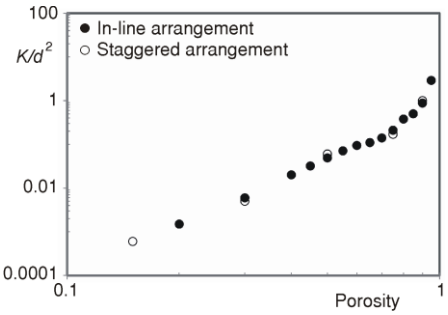

Figure 5. Logarithmic plot showing the dependence of the dimensionless permeability (K/d^2) on the porosity

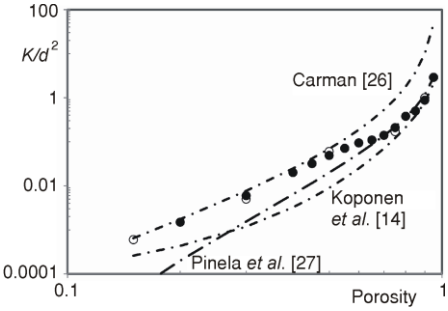

Figure 6. Comparison of K/d^2 obtained from the computational simulations with correlations available in the literature

Figure 3 also reveals that the effect of geometry (*i. e.*, in-line and staggered arrangements) is only significant outside the linear (Darcy's regime) flow. This means that, for a uniform distribution of cylinders in a 2-D porous structure, the arrangement does not affect the intrinsic permeability (fig. 5). The results of computational simulations depicted in fig. 5 also corroborate numerous studies available in the literature which display a strong dependence of the permeability on the porosity [13-17].

In fig. 6 we compare the dimensionless permeability generated by the computational simulations with the permeability obtained from the correlations developed by Koponen *et al.* [14], Kozeny *et al.* [26] and Pinela *et al.* [27]. This plot shows that the Kozeny-Carman correlation is consistent with our data only when the porosity is less than 0.55 (*i. e.*, for larger porosities this correlation overestimates our data). On the other hand, the result obtained from the simulations is significantly different from the values estimated with the correlations presented by Koponen *et al.* [14] and Pinela *et al.* [27] for low porosities but is in good agreement when the porosity is larger than 0.8 and 0.65, respectively. All three correlations present very poor estimation ability for porosities between 0.55 and 0.7.

The result depicted in fig. 5 shows that our data approximately coalesces into one exponential curve in the entire porosity domain. Therefore, the points can be fitted with the following equation:

$$\frac{K}{d^2} = 0.0003\exp(9.0956\varphi) \quad (r^2 = 0.976) \quad 0.25 \le \phi \le 0.95 \tag{15}$$

Figure 7 illustrates the dependence of the dimensionless inertia parameter λ on both the porosity and solid matrix arrangement. In contrast to the permeability results (fig. 5), λ is higher in the staggered arrangement than in in-line arrangement. Besides, the inertia parameter decreases with the void fraction (porosity). This result corroborates numerous data available in the literature (see for example [1, 2]) which display a strong dependence of porosity.

The inertia parameter λ obtained in these simulations is compared to the correlations suggested by [28, 29] in fig. 8. The plot shows that the Ergun's correlation agrees only for the in-line porous arrangement with porosity less than 0.8. It is also observed that the correlation

presented by Miguel [28] is found to agree only with the staggered porous arrangement for porosities between 0.3 and 0.6. It is noteworthy that both correlations produce very poor estimation of λ for a porosity larger than 0.6, independently of the arrangement.

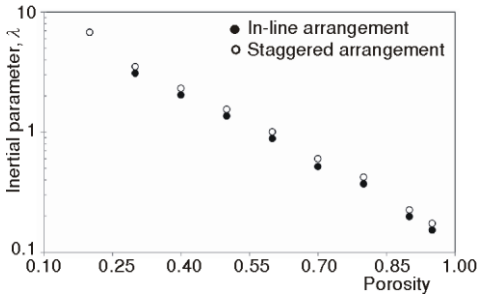

Figure 7. Logarithmic plot showing the dependence of the dimensionless inertial parameter λ on the porosity

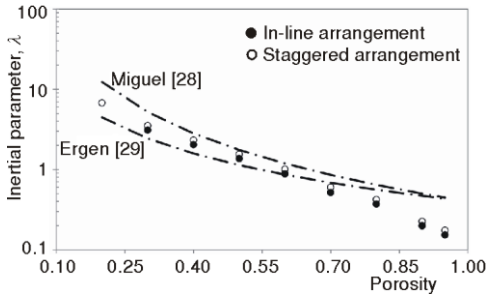

Figure 8. Comparison of λ obtained from the computational simulations with correlations available in the literature

According to fig. 7, the permeability generated by the computational simulations can be fitted with the following equation:

$$\lambda = c_\lambda \left(\frac{\varphi}{1-\varphi} \right)^{-0.867} \tag{16}$$

with

$$c_\lambda = 1.42 \quad (r^2 = 0.977) \quad 0.20 \le \phi \le 0.95 \qquad \text{for a staggered arrangement} \tag{17}$$

$$c_\lambda = 1.62 \quad (r^2 = 0.978) \quad 0.25 \le \phi \le 0.95 \qquad \text{for an in-line arrangement} \tag{18}$$

This result shows that the coefficient c_λ for a staggered arrangement is 12% higher than for an in-line arrangement.

Slip flow ($0.001 < Kn \le 0.1$): permeability vs. Knudsen number

Figure 9 is a summary of the results obtained for the dimensionless permeability in the slip-flow regime. This plot shows that the K/d^2 depends not only on the porosity but also both on the Knudsen number and the arrangement of the solid matrix. Although the porosity dependence is similar for both no-slip and slip-flow regimes (*i. e.*, the permeability increases with the porosity), the effects of Knudsen number and solid matrix arrangement are different. For a no-slip flow regime, K/d^2 is not dependent of both Kn and matrix arrangement. On the other hand, for a slip-flow regime, dimensionless permeability is higher for the in-line arrangement than for the staggered arrangement of the solid matrix. Besides, the dimensionless permeability, K/d^2, follows a power-law increase with the Knudson number (*i. e.*, $K/d^2 \sim \mathrm{Kn_o}^{0.45}$ and $K/d^2 \sim \mathrm{Kn_o}^{0.23}$ for porosities of 0.3 and 0.5, respectively).

Notice that both K/d^2 and the Knudsen number (eq. 10) depicted in fig. 9 are dependent on the characteristic dimension, d, of the solid matrix. Therefore, to obtain a further insight into the dependence of intrinsic permeability on the Knudsen number, the ratio of the intrinsic permeability to the distance of the mean-free path, K/l^2, *vs.* the Knudsen number is depicted in fig. 10. If l = constant, this dimensionless permeability follows a power-

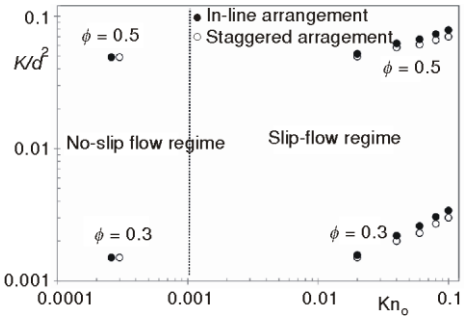

Figure 9. Logarithmic plot showing the dependence of the dimensionless permeability (K/d^2) on the Knudsen number

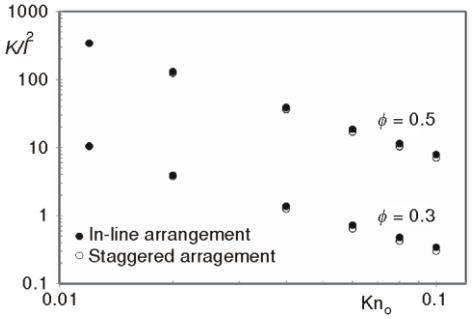

Figure 10. Logarithmic plot showing the dependence of the ratio of intrinsic permeability to distance of the mean-free path (K/l^2) on the Knudsen number

law decrease with the Knudson number (*i. e.*, $K/l^2 \sim \mathrm{Kn_o}^{-1.6}$ and $K/l^2 \sim \mathrm{Kn_o}^{-1.8}$ for porosities of 0.3 and 0.5, respectively). This tendency agrees with the results reported by Miguel *et al.* [5].

Conclusions

The LBM with the D2Q9 model was applied to solve non-Darcy flow through 2-D porous media. Staggered and in-line arrangements of uniform cylinders were considered. Our simulation results were presented in terms of a friction factor and are compared to dimensionless Darcy-Forchheimer equation, a widely used model for porous media. Results show that Darcy-Forchheimer equation is successfully correlated with the data of our simulations. Besides, the permeability and the inertial parameter are obtained from the best fit of these data. New insights and correlations for the relationship between these parameters and the porosity are presented.

Simulations are also carried out for both no-slip and slip-flow regime. The effect of the staggered and in-line arrangements on the permeability is studied. The relationship between the intrinsic permeability and the Knudsen number is studied. For non-slip flow conditions the permeability doesn't depend on the Knudsen number. On the other hand, the permeability follows a power-law variation with the Knudson number for slip-flow regime.

In summary, the present study reveals many interesting features of flow through porous structures and demonstrates the capability of the LBM to capture these features both in no-slip and slip flow regime.

Acknowledgments

Thanks are due to Dr. Z. Lee for his collaborative support on LBM simulations.

Nomenclature

c_s – sound speed, [ms^{-1}]
d – characteristic length of the flow geometry, [m]
$\mathrm{Fo_K}$ – Forchheimer number, [–]
f_K – friction factor, [–]
$f_i^{(0)}$ – equilibrium distribution function, [–]
K – permeability, [m^2]
Kn – Knudsen number, [–]
k_B – Boltzmann constant, [JK^{-1}]
L – thickness of the porous media, [–]

l – mean free path, [m]
m – molecular mass, [kg]
p – pressure, [Pa]
Re_K – Reynolds number based on permeability, [–]
r – position, [m]
T – temperature, [K]
t – time, [s]
u – velocity, [ms^{-1}]
u_{mol} – molecular velocity, [ms^{-1}]
v_i – velocity point in direction e_i, [ms^{-1}]

Greek symbols

β – inertial coefficient, [m^{2}s^{-1}]
λ – dimensionless inertia parameter, [–]
ν – equivalent viscosity
ρ – fluid density, [kg m^{-3}]
τ – dimensional relaxation time, [–]
ϕ – porosity
χ – lattice number in the geometry, [–]
Ω_i – collision operator, [–]

Subscripts

i – labels the lattice directions
o – outlet

References

[1] Vafai, K., Handbook of Porous Media. Marcel Dekker, New York, USA, 2000
[2] Nield, D., Bejan, A., Convection in Porous Media. Springer, New York, USA, 1998
[3] Beskok, A., Karniadakis, G. E., Simulation of Heat and Momentum Transfer in Complex Microgeometries, *J. Thermophys. Heat Transfer, 8* (1994), 4, pp. 647- 65
[4] Karniadakis, G. E., Beskok, A., Microflows: Fundamentals and Simulation. Springer, New York, USA, 2002
[5] Miguel, A. F., Serrenho, A., On the Experimental Evaluation of the Permeability in Porous Media Using a Gas Flow Method, *Journal of Physics D, 40* (2007), 21, pp. 6824-6828
[6] Beskok, A., Karniadakis, G. E., A Model for Flows in Channels, Pipes, and Ducts at Micro and Nano Scales, *Microscale Thermophys. Engng, 3* (1999), 1, pp. 43-77
[7] Succi, S., The Lattice Boltzmann Equation for Fluid Dynamics and Beyond. Oxford University Press, Oxford, UK, 2001
[8] Pan, C., Luo, L.-S., Miller, C. T., An Evaluation of Lattice Boltzmann Schemes for Porous Medium Flow Simulation, *Computers & Fluids*, 35 (2006), 8-9, pp. 898-909
[9] Qian, Y. H., D'Humieres, D., Lallemand, P., Lattice-BGK Models for Navier-Stokes Equation, *Europhys. Lett., 17* (1992), 6, pp. 479-484
[10] He, X., Luo, L. S., Theory of the Lattice Boltzmann Method: From the Boltzmann Equation to the Lattice Boltzmann Equation, *Phys. Rev. E, 56* (1997), 6, pp. 6811-6817
[11] Chen, F., *et al*., Multiple-Relaxation-Time Lattice Boltzmann Model for Compressible Fluids, *Physics Letters A, 375* (2011), 21, pp. 2129-2139
[12] Lallemand, P., Luo, L.-S., Theory of the Lattice Boltzmann Method: Dispersion, Dissipation, Isotropy, Galilean invariance, and Stability, *Phys. Rev. E, 61* (2000), 17, pp. 6546-6562
[13] Jeong, N., Choi, D. H., Lin, C.-L., Estimation of Thermal and Mass Diffusivity in a Porous Medium of Complex Structure Using a Lattice Boltzmann Method, *International Journal of Heat and Mass Transfer, 51* (2008), 15-16, pp. 3913-3923
[14] Koponen, A., *et al*., Permeability of Three Dimensional Random Fiber Web, *Physics Review Letters, 80* (1998), 4, pp. 716-719
[15] Manwart, C., *et al*., Lattice-Boltzmann and Finite-Difference Simulations for the Permeability for Three-Dimensional Porous Media, *Phys. Rev. E, 66* (2002), 1, pp. 016702
[16] Wu, H. R., *et al*., Lattice Boltzmann Simulation of Flow in Porous Media on Non-Uniform Grids, *Progress in Computational Fluid Dynamics, 5* (2005), 1-2, pp. 97-103
[17] Jeong, N., Choi, D. H., Lin, C.-L., Prediction of Darcy-Forchheimer Drag for Micro-Porous Structures of Complex Geometry Using the Lattice Boltzmann Method, *J. Micromech. Microeng., 16* (2006), 10, pp. 2240
[18] Mendoza, M., Wittel, F. K., Herrmann, H. J., Simulation of Flow of Mixtures through Anisotropic Porous Media Using a Lattice Boltzmann Model, *European Physical Journal E, 32* (2010), 4, pp. 339-348
[19] Rivet, J. P., Boon, J. P., Lattice Gas Hydrodynamics, Cambridge University Press, Cambridge, UK, 2001

[20] Dunweg, B., Schiller, U. D., Ladd, A. J. C., Statistical Mechanics of the Fluctuating Lattice Boltzmann Equation, *Phys. Rev. E*, *76* (2007), 3, pp. 036704
[21] Chopard, B., Droz, M., Cellular Automata Modelling of Physical Systems, Cambridge University Press, Cambridge, UK, 1998
[22] Kim, J., Lee, J., Lee, K. O., Nonlinear Correction to Darcy's Law for a Flow Through Periodic Arrays of Elliptic Cylinders, *Physica A, 293* (2001), 1-2, pp. 13-20
[23] Serrenho, A., Miguel, A. F., Simulation and Characterization of High Porosity Media for Aerosol Particle Processing, *Journal of Porous Media*, *12* (2009), 12, pp. 1129-1138
[24] Miguel, A. F., *et al.*, Wind-Induced Airflow Through Permeable Materials: Part I, *Journal of Wind Eng. and Ind. Aerodynamics*, *89* (2001), 1, pp. 45-57
[25] Serrenho, A., Miguel, A. F., Fluid Flow and Solid/Fluid Suspensions Flow in 3-D Packed Beds of Spheres: the Effect of Periodicity of Fixed Beds, *Defect and Diffusion Forum, 312-315* (2011), April, pp. 871-876
[26] Carman, P. C., Flow of Gases through Porous Media, Butterworths, London, 1956
[27] Pinela, J., *et al*., Permeability-Porosity Relationship Assessment by 2D Numerical Simulations, *Proceedings*, 16th International Symposium on Transport Phenomena, Prague, 2005
[28] Miguel, A. F., Airflow through Porous Screens: From Theory to Practical Considerations, *Energy and Buildings*, *28* (1998), 1, pp. 63-69
[29] Ergun, S., Fluid Flow through Packed Columns, *Chem. Engng. Prog.*, *48* (1952), 2, pp. 89-94

Paper submitted: September 29, 2010
Paper revised: January 8, 2012
Paper accepted: January 16, 2012